Soft Matter

PAPER

View Article Online
View Journal | View Issue

Cite this: *Soft Matter*, 2026, **22**, 3403

The effect of weathering environments on microplastic chemical identification with Raman and IR spectroscopy: Part II. polystyrene, polyethylene terephthalate, and nylon 6

Samantha Phan, †[a] Jonathan J. Ramtahal †[b] and Christine K. Luscombe †*[c]

The use of spectroscopic techniques to identify microplastics found in the environment is challenging because weathered microplastics undergo chemical changes that make their spectra drastically different from their pristine counterparts. In previous work, we reported the findings from systematic artificial weathering of polyethylene and polypropylene for 0–26 weeks in four different weathering environments (air, DI water, artificial seawater, and Puget Sound seawater), characterized by Raman and IR spectroscopy (https://doi.org/10.1016/j.polymertesting.2022.107752). This manuscript provides the final part of the study's findings, which includes the Raman and IR spectroscopy information on the weathering effects on polystyrene (PS), polyethylene terephthalate (PET), and nylon 6 (PA6) with the goal to evaluate how these weathering effects affect the reliability of polymer identification. Our results show that spectral changes are often non-linear, lacking a clear exposure-time trend. While PS exhibited significant oxidation by IR in DI water, these changes were not detectable by Raman spectroscopy, highlighting a risk for researchers who rely on a single technique. Both PS and PA6 showed more degradation peaks in DI water than in seawater, which suggests that chlorine radicals from salt may inhibit the formation of some degradation products. This work underscores the need to use complementary IR and Raman analysis to avoid misinterpretation of environmental microplastics and their aging state.

Received 4th November 2025,
Accepted 6th April 2026

DOI: 10.1039/d5sm01102g

rsc.li/soft-matter-journal

Introduction

Plastics are designed to be durable and withstand harsh environmental conditions while maintaining their structural integrity and performance. This property, however, has allowed plastics to persist in the environment for much longer than their intended lifetimes, resulting in the widespread presence of plastic pollution and microplastics, defined as plastic particles <5 mm in size.[1–3] When microplastics enter the environment, they are further modified, which result in microplastics with varying degrees of chemical modification and morphological changes compared to their material source. In the environment, conditions such as exposure to UV radiation, heat, wind, and wave motion facilitate the breakdown and fragmentation of larger items into microplastics that can interact with marine organisms[4–6] and potentially affect human health.[7] Weathering of microplastics can lead to fragmentation, leaching of plasticizers,[8] and increased mobility of harmful chemicals.[9] It was estimated that in 2016, 19–23 million metric tons, or 11%, of plastic waste generated globally entered aquatic ecosystems, which may increase to 53 million metric tons by 2030.[10]

Environmental weathering of microplastics is a complex process and is influenced by climate, regional conditions, and many other factors that are difficult to control in the laboratory.[11] The major processes involved in plastic degradation can differ depending on the conditions in which plastics are found and must be understood to assess potential hazards.[11,12] Microplastic degradation can be owed to both mechanical and chemical processes which can be summarized as follows: (1) photodegradation – the action of light, (2) thermooxidation – slow oxidative breakdown at moderate temperatures, (3) thermal degradation – action at high temperatures (industrial or environmental), (4) hydrolysis – reaction with water, and (5) biodegradation – the action of organisms (*i.e.*, microbes).[13] In the natural environment, these different processes of degradation act in collaboration and in interaction with each other, with photodegradation as the main process.[13] Depending on the functional groups present in a polymer, this can lead to a myriad of reactions and

[a] *Department of Chemistry, University of Washington, Seattle, WA 98195, USA*
[b] *Shimoda Marine Research Center, University of Tsukuba, Shimoda 5-10-1, Shizuoka, 415-0025, Japan*
[c] *Department of Materials Science and Engineering, University of Washington, Seattle, WA 98195, USA*
† Current address: pi-Conjugated Polymers Unit, Okinawa Institute of Science and Technology, Onna, Okinawa 904-0495, Japan. E-mail: christine.luscombe@oist.jp

processes that result in many different chemical changes and byproducts.

The accurate identification of environmental microplastics remains a major methodological challenge mainly because of the diversity of polymers coupled with the various physicochemical changes as a result of environmental weathering. Many studies rely on visual identification and sorting microplastics from non-plastic materials. Although rapid and cost-effective, these methods often introduce misidentification, leading to systematic over or under estimation of microplastic concentration. Spectroscopic techniques including Raman microspectroscopy (μ-Raman) and Fourier transform infrared microspectroscopy (μ-FTIR) are robust non-destructive methods that can be employed for polymer confirmation. While more reliable than visual identification, a major limitation of these methods lies in the availability and quality of comprehensive spectral libraries.[4,5,13–16] Environmentally weathered microplastics often exhibit altered functional groups, surface oxidation, and physical degradation relative to pristine polymers. Such alterations greatly reduce spectral matching reliability. This is further complicated when attempting to separate microplastics from their environmental matrices and measurement of significantly weathered microplastic surfaces.[17,18] Researchers are working to incorporate weathered spectra into libraries,[4,5,8,9] but this is complicated by the fact that environmental degradation is far more complex than laboratory simulations can effectively replicate.

Previously, we began to address this lab-to-environment gap by studying polyethylene (PE) and polypropylene (PP).[15] We found that they show variations in crystallinity and oxidative byproducts depending on the weathering condition (air, DI water, artificial seawater, and Puget Sound seawater), with samples in Puget Sound seawater showing the greatest changes. However, polyolefins such as PE and PP are not the only polymers commonly found in the environment. To expand the understanding of the effect of varying weathering conditions on IR and Raman spectral changes to other common polymer types, here, we present the remaining weathering results of polystyrene (PS), polyethylene terephthalate (PET), and nylon 6 (PA6) and elaborate on the complexities of their spectral changes.

Experimental

Materials

All plastic samples used in this study were purchased in pure form from Sigma-Aldrich, used unaltered, and measured with a ruler to confirm their size. It is noted that even in these research-grade materials, minor spectral features consistent with residual stabilizers (*e.g.*, phosphite antioxidants in PET) were detectable. PS pellets were sized from 3 to 5 mm with an M_w of 35 000 and a density of 1.06 g mL^{-1}. PET pellets were about 4 mm in size and had a density of 1.68 g mL^{-1}. PA6 pellets were about 3 mm in size and had a density of 1.084 g mL^{-1}. The M_w value of PS was provided by Sigma-Aldrich, but values for PET and PA6 pellets were not reported. Sea salts (NutriSelect® Basic) were purchased from Sigma-Aldrich as an artificial seawater mix. Water, collected directly from the surface of the Puget Sound (47.616844, 122.358928) in a glass container without any filtration or treatment, was also used for the studies within 24 h of collection.

Experimental procedure

This study aimed to investigate the influence of sunlight and different types of water on microplastic weathering without mechanical abrasion at ambient temperatures. More details on the experimental procedure can be found in our previous work, which investigated the same weathering conditions and reported the results for PE and PP.[15] Six plastic pellets of each polymer type (PET, PS, and PA6) were placed into 20-mL glass vials with three replicants of each vial sample type and exposed to one of four weathering conditions: empty (air), deionized water, artificial seawater, or Puget Sound seawater. Artificial seawater solution was made with 35 g of NutriSelect® Basic and 1 L of DI water according to instructions provided by the suppliers. The salinity of artificial seawater (35 ppt) was similar to the salinity of the Pacific Ocean (34 ppt).[19–21] Due to tidal current mixing, the salinity of the Puget Sound averages around 29 ppt. Vials were filled with 15 mL of each type of water and sealed with a glass coverslip to prevent foreign particles from entering the vials and to reduce water evaporation. The vials were then placed on an automatic rocker (Ohaus™ 2 Tier Rocking Shaker) to mimic light ocean waves. Thermometers were regularly used to ensure that the air temperature remained within the range of 25–30 °C. The average temperatures of the Puget Sound can range from 5 °C in the colder months to 19 °C in the warmer months and reach peaks of 24 °C in August.[22]

The light source for solar irradiation was Tungsten halogen Solux 4700 K light bulbs, which were chosen to match the AM1.5 solar spectrum at 25 °C.[23,24] The 4700 K tungsten halogen Solux lamps were used by Reese *et al.* to test photo-induced degradation of polymer and polymer–fullerene active layers in photovoltaics, and comparative data of the lamp used for illumination conditions relative to AM1.5G are available in the SI (Fig. S1).[23] Subsequently, Holliday and Luscombe used the same lamp to investigate photooxidative stability in organic photovoltaics.[24] On clear, cloudless days, the solar irradiation is 1000 W m^{-2}; however, this value is greatly influenced by angle, organisms, water vapor, suspended particles, *etc.*[15] The lightbulbs were positioned as in the study of Phan *et al.*, 11 cm from the edge of the top tray and 16 cm above the top of the tray.[15] The lightbulbs were connected to a lightbulb socket, a transistor, and a mechanical timer that allowed 12 h of continuous light irradiation and 12 h without irradiation to mimic a typical day. The radiance on the vials ranged from 85 to 159 W m^{-2}, depending on the vial location, which was measured with a Topcon spectroradiometer. The vials were regularly rotated and monitored to ensure that all samples received the same average light exposure and that the temperatures remained at 25–30 °C over the 26 weeks. The glass vials were sufficient to allow all wavelengths of light to pass. One aliquot pellet of each sample was taken out every 2 weeks for 10 weeks and then at 26 weeks

of irradiation to observe any long-term changes. Each aliquot was rinsed with copious amounts of DI water (especially for samples exposed to salt water), placed in a vial, and dried in a desiccator at room temperature before characterization. Spectra were taken on multiple points on any given pellet to provide statistically meaningful data.

Instrumentation and processing

Raman characterization was conducted with a Renishaw inVia Raman microspectrometer equipped with a 785 nm laser with 10× and 50× objectives to focus the laser on the microplastic surface. All measurements were conducted for 5 accumulations at 5% laser power. Additional Raman characterizations with a 532 nm laser and a 100× objective were conducted with a WiTec alpha300 Apyron Raman microspectrometer. The spectra were subjected to data processing depending on the signal-to-noise ratio and fluorescent interference (which produced a curved, sloped baseline). Baseline correction was completed using the default parameters (λ = 100, p order = 1, repetitions = 15) of the reweighted penalized least squares algorithm developed by Zhang *et al.* to create a consistent baseline correction and avoid microscope objective interference signals.[25] The processed Raman spectra were normalized to a reference peak that was known to be consistent regardless of polymerization or degradation. In PS, the 1002 cm^{-1} peak was used as it represents the benzene breathing mode.[26,27] PET was normalized to 1291 cm^{-1}, which corresponds to the C–O and ring stretch.[28,29] PA6 was normalized to 1126 cm^{-1}, a C–C skeletal stretching mode.[30] Spectral deconvolution was performed by an automatic fitting algorithm provided by MagicPlot using mixed Gaussian and Lorentzian curves,[31,32] which was used to calculate carbonyl indices and spectral intensity ratios. Representative deconvoluted spectra are shown in Fig. S2–S4.

Results and discussion

Polystyrene

PS is a major commodity plastic often used in single-use products. Its structure, which contains a phenyl group, allows for strong UV absorption. Raman spectroscopy has previously revealed photodegradation in such structures by tracking changes in aromatic and aliphatic peaks.[33] However, a striking result of our study was that even with increasing light exposure time, the weathered PS revealed no significant difference in the Raman spectra in any weathering condition, and all signature PS peaks were easily identifiable (Fig. S5 and Table S1).

Our results contrast with previous studies[33] in which Raman peak changes in PS, exposed to natural sunlight at higher temperatures (35.8–37.4 °C), were observed. This discrepancy likely highlights the influence of experimental conditions, as elevated temperatures and different irradiance levels can lead to different chemical reactions during degradation.[34–37] Another difference was the instrumentation: our study used a 785 nm laser, while Kilinc *et al.* used a 532 nm laser.[33] Chemical modification can occur to varying degrees on the surface and in the bulk. We hypothesized that our laser's deeper penetration (12 μm for 785 nm *vs.* 0.7 μm for 532 nm)[38,39] might obscure surface changes. However, our additional characterizations with a 532 nm laser source still revealed no significant differences (Fig. S6), confirming our initial finding.

In the context of the Puget Sound, where one of the water samples for weathering was taken, this region receives significant cloud coverage throughout the year, which decreases the solar irradiance and slows environmental photodegradation.[40] The irradiance in Kilinc *et al.*'s[33] study ranged between 791 W m^{-2} and 890 W m^{-2}, which is 6–9 times higher than the irradiance in this study. It is likely that the level of light exposure to the PS samples in this study, though similar to the environment of the Puget Sound, is insufficient to induce any observable changes to the Raman spectra. This is particularly interesting because Raman measurements of PS extracted from marine organisms,[4,5] from the Puget Sound, also showed that the Raman spectra of PS were similar to reference spectra of PS with few appearances and no disappearances of characteristic Raman spectral peaks, while other polymers, such as PP, nylon, and PET, show more spectral variances. This demonstrates the importance of investigating different weathering conditions on the chemical changes of microplastics to ensure adequate plastic identification.

In contrast to Raman, IR spectroscopy revealed the various peaks associated with oxidative functional groups, such as OH, C–O, and C═O groups, when PS was subjected to increasing light exposure and appeared in all the different weathering conditions (Fig. 1). In weathered PS, the formation of a band around 3464 cm^{-1} and an intensity increase at 1745 cm^{-1} indicated the formation of hydroperoxy and carbonyl groups, respectively.[41] The phenyl ring in PS can be excited and, through intersystem crossing, form a triplet state under UV radiation.[12] That triplet energy can be transferred to nearby C–H or Ph–C bonds.[11,12,14] The cleavage of those bonds can form polystyryl radicals, which are converted to peroxy radicals that participate in crosslinking and chain scission, resulting in the formation of ketones, styrene monomers, and olefins.[11,14]

In contrast to the single new peak at 1410 cm^{-1} in the air-weathered IR spectra, samples weathered in water showed broad bands around 3350 cm^{-1} and between 1745 cm^{-1} and 826 cm^{-1}. These findings suggest the formation of diverse, oxidized species for the water samples (Table 1 and Fig. 1). All water conditions showed hydroxyperoxide formation (bands 3390–3232 cm^{-1}), supported by peaks around 1300 cm^{-1}.[15,41] Hydroxyperoxides, also seen in weathered PP, act as major sources of free radicals during photodegradation.[15,42]

Upon closer examination of the IR spectra of PS samples weathered in water, PS weathered in DI water exhibited the most unique peaks (1664, 1547, 1372, 1344, 1280, 1242, and 826 cm^{-1}) compared to PS weathered in the other water conditions. This suggests that PS weathered in DI water may differ from other the weathering conditions resulting in the production of C═O, O–O, and C–O bond-containing byproducts. Though beyond the scope of this study, an in-depth mechanism analysis regarding the effects of water molecules on the free radical reaction pathways of PS degradation will be

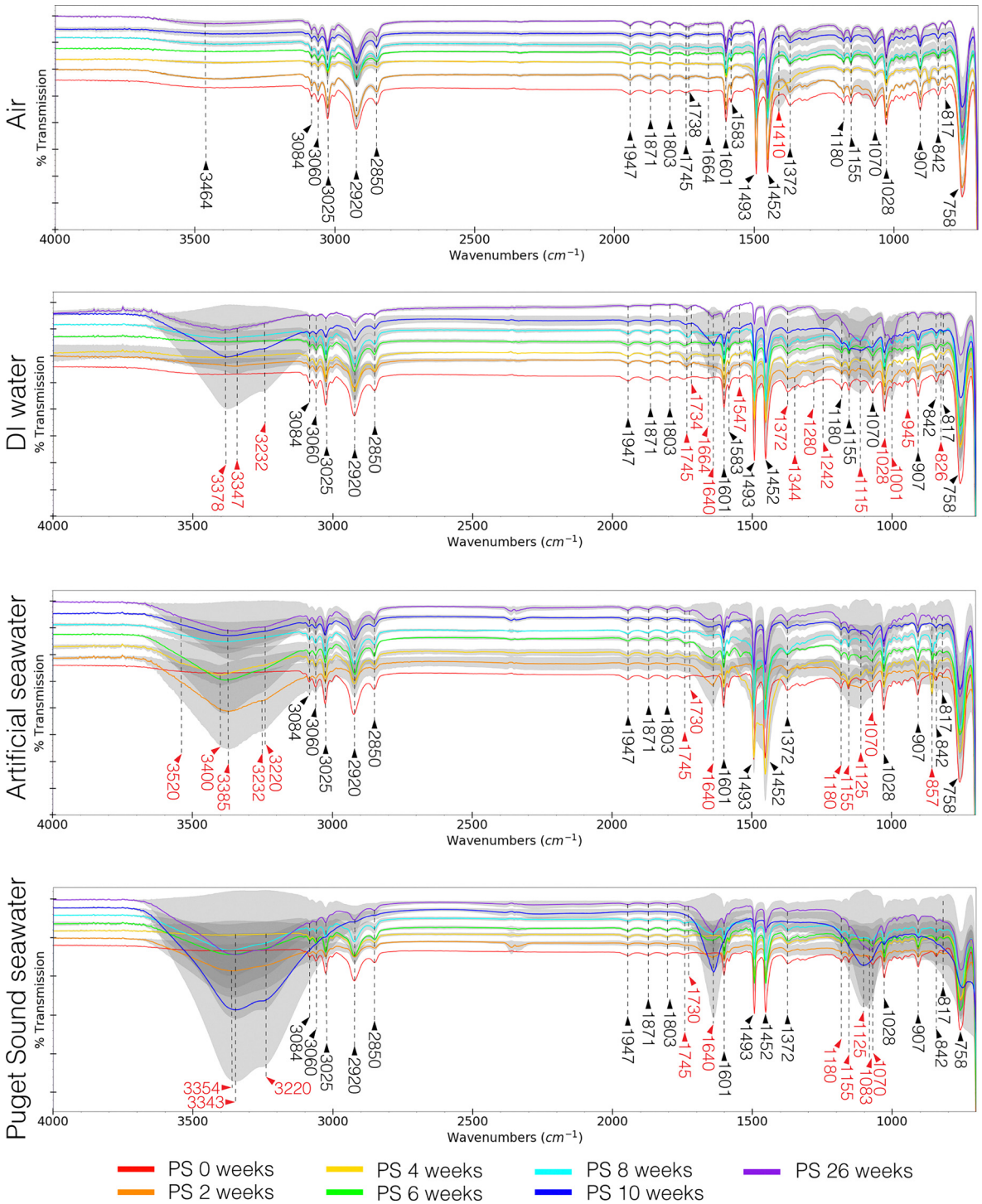

Fig. 1 Average IR spectra and standard deviations (grey error bands) of PS over time in four different weathering conditions in a staggered overlay. Red peaks are new IR peaks that differ from pristine PS.

useful in elucidating the origin of the oxidative peaks in DI water. The IR spectrum of PS weathered for 10 weeks in Puget Sound seawater appears similar to pristine PS. This could indicate some flaking of the PS surface, similar to PE,[15,43] as weathered PS also showed surface cracking (Fig. 2). Another explanation is that salinity has a greater influence on the weathering for PS, as the functional group formation for PS weathered in artificial seawater and Puget Sound seawater is similar, but different for PS weathered in DI water.

In seawater, NaCl contributes to about 90% of its salinity concentration.[44] The Cl^- in seawater can inhibit the photo-aging of microplastics because reactive chlorine radicals ($Cl_2^{\bullet -}$)

Table 1 Selected IR peaks and associated vibrational modes of PS

Peak position (cm^{-1})	Vibrational mode	Weathering condition			
		Air	DI	AS	PSS
3520, 3464, 3400, 3347, 3220[a]	R–O–OH[15,57]		×	×	×
3550–3220[a]	O–H stretch[41,57]		×	×	×
3084, 3060, 3025	Aromatic CH stretch[46,58,59]	×	×	×	×
2920, 2850	CH_2 asymmetric and symmetric stretch[46,58]	×	×	×	×
1745,[a] 1730[a]	C=O stretch[41]		×	×	×
1664[a]	C=C stretch[47]		×		
1640[a]	C=C or C=O[43]		×	×	×
1601, 1493, 1452	Aromatic ring modes[46,58,59]	×	×	×	×
1344[a]	Unknown		×		
1280,[a] 1242[a]	C–O stretch[41]		×		
1115[a]	Aromatic skeleton and C–O stretch[60,61]		×	×	×
1080[a]	C–O, phthalate, secondary alcohol[41,46]				×
857[a]	C–H wag, *para*-substituted aromatic[46]			×	
826[a]	C–H wag, *meta*-substituted aromatic[46]		×		
758	Aromatic out-of-plane CH bend[58]	×	×	×	×

DI = deionized water, AS = artificial seawater, PSS = Puget Sound seawater. [a] Indicates peak changes.

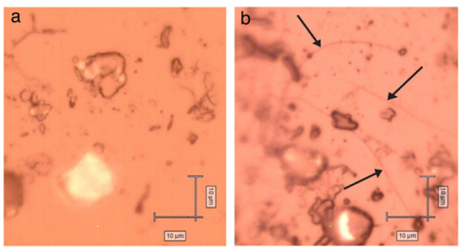

Fig. 2 Optical microscopy images of (a) pristine PS and (b) weathered PS in PSS for 26 weeks. Weathered PS exhibited long propagating cracks (indicated by the arrows) while pristine PS exhibited no cracks. Both pristine and weathered PS have irregularities on their surfaces and are not smooth. Scale bar indicates 10 μm.

could quench perhydroxyl radicals ($HO_2^{\bullet}$).[45] With perhydroxyl radicals quenched, the free radical chain reaction under light irradiation would be inhibited, which explains the fewer unique peaks in PS weathered in the seawater conditions. In DI-water weathered PS, various C=C bonds were observed (Table 1), which indicates that chain scission resulted in the formation of different olefins. The intensity changes in the peaks around 3400 cm^{-1} and 1640 cm^{-1} in PS weathered in the water conditions were much greater than those observed in PS weathered in air. Unique to PS weathered in the Puget Sound seawater was the formation of a peak at 1080 cm^{-1}, which indicates a C–O stretch from a secondary alcohol.[41,46] The formation of more unique IR peaks for DI water-weathered PS compared to the Puget Sound seawater-weathered PS is a notable difference from previous findings for weathered PP, where PP weathered in Puget Sound seawater showed more peaks associated with C–O–C and O–O stretches between 1300 and 900 cm^{-1}.[15] PP weathered in Puget Sound seawater also exhibited the formation of unique hydroperoxides compared to the other weathering conditions, along with groups indicative of crosslinking and chain scission that resulted in increased crystallinity in the weathered samples.

While the contradictory results for PP and PS may be due to their different chemical structures, another possibility is the role of microbial action. PS is known to release toxic aromatic VOCs during degradation, which could inhibit microbial activity.[47–49] In contrast, the byproducts of PP may be less toxic, potentially allowing for microbial degradation to occur. This study did not analyze VOCs or microbial composition, so this remains a hypothesis that warrants future investigation.

The degree of weathering can be monitored by the carbonyl index (CI),[50] the ratio of the carbonyl band and the reference band, which, in the case of PS, is the CH_2 stretching band.[51,52] The CI for PS can be calculated by eqn (1):

$$CI_{PS} = \frac{A_{1745}}{A_{2850}} \quad (1)$$

where A_{1745} is the IR absorbance at 1745 cm^{-1} and A_{2850} is the IR absorbance at 2850 cm^{-1}. The CI of PS with increasing light exposure in all the environments was highly variable and only slightly increased over time in all weathering conditions (Fig. S7). In some cases, weathering in artificial seawater and Puget Sound seawater showed large bands that obscured the peak at 1745 cm^{-1}, therefore the CI could not be calculated for those trials. The presence of oxygen-containing functional groups suggests that the PS was oxidized (Table 1), while the presence of C=C bonds indicates the cleavage of the polymer chain.[53] The degradation of PS has been reported to occur in two stages, where Stage I is dominated by photooxidation in the near-surface layer, followed by Stage II, where microcrack formation and particle rupture accelerate degradation.[54] As such, the fluctuation of the CI may be due to the repeated photooxidation and then cracking or flaking of the PS surface, which then results in the exposure of less weathered PS (Fig. 2).[55,56]

These findings for PS highlight a methodological challenge. While Raman spectroscopy was unaffected by weathering, similar to our findings for PE and PP, it failed to detect the significant oxidation that occurred. Conversely, IR spectroscopy did detect this oxidation, but in severe cases, these new weathering bands obstructed polymer identification. For example, PS weathered for 26 weeks in Puget Sound seawater showed strong weathering bands (around

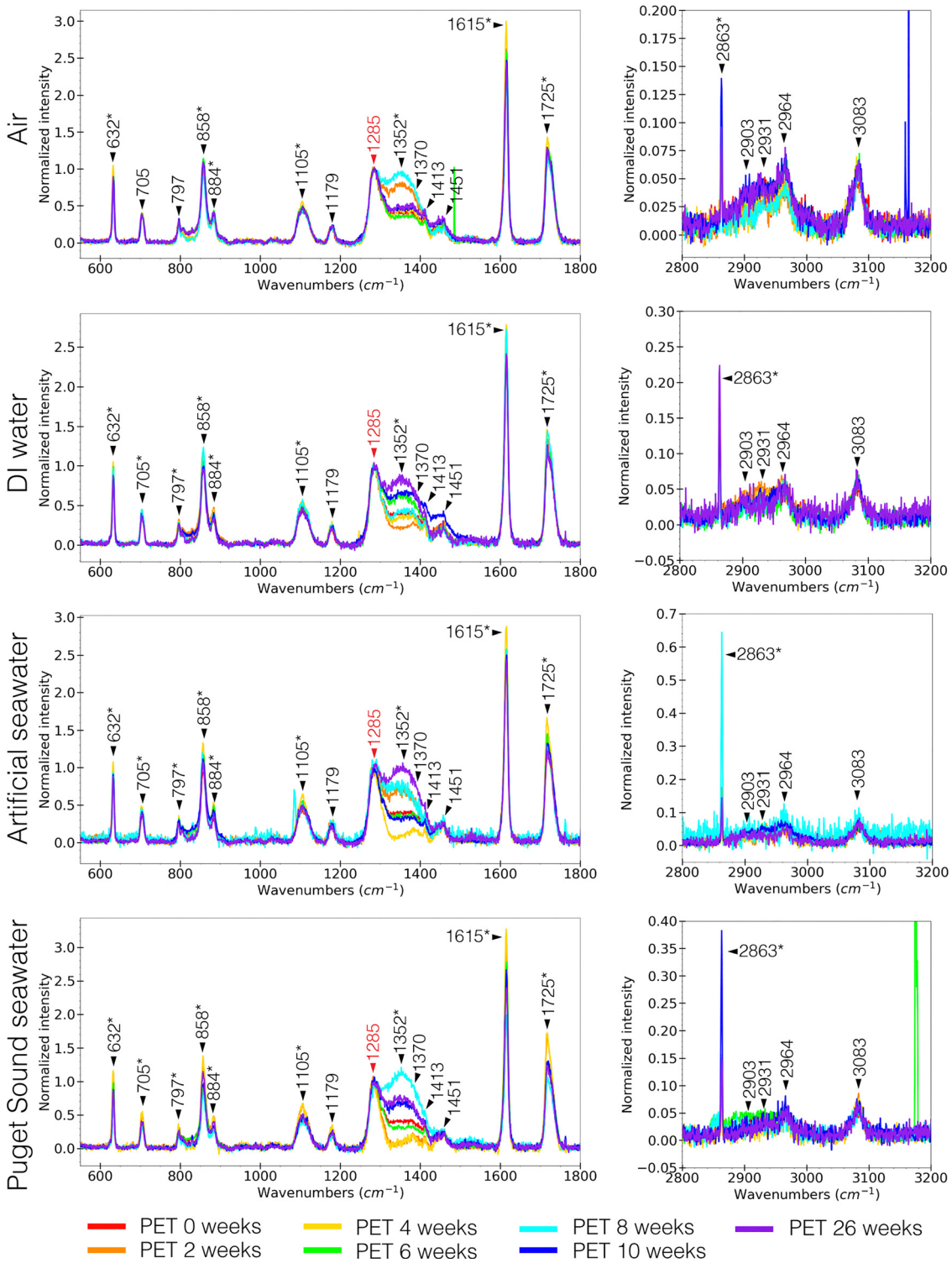

Fig. 3 Truncated Raman spectra highlighting the PET Raman spectral regions that exhibit the greatest normalized variability over time and in different weathering conditions (air, DI water, artificial seawater, and Puget Sound seawater). Red peak was used in spectral normalization. Asterixis-marked peaks showed the most observable changes.

3250, 1640, and 1100 cm^{-1}) that obscured the polymer's identifying IR peaks. Artificial seawater samples showed similar, albeit less intense, bands. This presents a challenge for single-method analyses: Raman may falsely identify the plastic as pristine, while IR may fail to identify the polymer at all. These results emphasize that relying on one technique can lead to false negatives and underestimation of microplastic pollution.

Polyethylene terephthalate

PET,[62] composed of aromatic rings and hydrolysable ester bonds, is susceptible to degradation. In sharp contrast to the Raman spectra of PS, PET exhibited a clear and consistent spectral change upon weathering: the appearance of a new Raman peak at 1352 cm^{-1} in all conditions (Fig. 3). This peak corresponds to the 'D band' found in carbonaceous material, which indicates an increase in structural disorder or defects in the polymer chain and represents the ring breathing modes of sp^2 carbon rings.[63,64] The G band, associated with ordered sp^2 graphene or graphitic materials,[55] was not observed. While all samples showed a change at 1352 cm^{-1}, our key finding is that PET samples weathered in air showed no obvious trend over time and the samples weathered in water exhibited an increasing normalized Raman intensity at 1352 cm^{-1} (Fig. 3 and Fig. S8), implying that weathering in water generates a more disordered structure at the surface. The normalized Raman intensity at 1352 cm^{-1} for PET had values of 0.58 (air), 0.64 (DI), 0.91 (artificial seawater), and 1.1 (Puget Sound seawater). The 1370 cm^{-1} peak corresponds to CH_2 wagging[64] but is overlapped by the 1352 cm^{-1} peak, which makes it challenging to attribute the intensity variations to specific structural changes in PET. Differences in peak intensity were also observed at the 632, 858, 884, 1105, 1615, 1725, and 2863 cm^{-1} peaks, which correspond to various C–C, C–O, and C–H vibrational modes (Table 2).

One common method to track PET crystallinity with Raman is to analyze the ratio between the 1097 cm^{-1} and 1120 cm^{-1} peaks, which correspond to the *trans* (crystalline) and *gauche* (amorphous) conformations of the ethylene glycol unit, respectively.[29,64,65] However, when we applied this analysis, our PET samples showed peak differences in this region, and the results were inconclusive. This may be due to water acting as a plasticizer, promoting chemi-crystallization in the amorphous regions.[66]

We therefore turned to another peak long associated with crystallinity: the C═O stretch at 1725 cm^{-1}.[67,68] We found that all weathering conditions exhibited fluctuations in this stretch, with Puget Sound seawater and artificial seawater weathering showing significantly more variability (Fig. 3 and Fig. S9). While higher crystallinity is known to narrow this peak, our samples in water conditions had similar peak widths to those weathered in air (Fig. S9). This suggests that the greater intensity variation in artificial seawater and Puget Sound seawater indicates a change in the C═O stretching moieties rather than a change in crystallinity.

Finally, we examined the 1615 cm^{-1} peak, where a decrease indicates more aligned benzene rings.[29,67] We observed minimal variations in air, DI, and artificial seawater, but slightly more variation in Puget Sound seawater. Taken together, these findings suggest that saltwater weathering (artificial seawater and Puget Sound seawater) alters C═O moieties and polymer backbone orientation, while Puget Sound seawater also increases structural disorder (as supported by the sp^2 carbon ring fluctuations).

IR spectroscopy is more sensitive to polar functional groups than Raman spectroscopy and is well-suited to elucidate oxidative functional groups formed during weathering. However, the IR spectra of PET weathered in all the conditions showed few peak changes and no disappearances of characteristic identification peaks (Fig. 4 and Table 3); this is a stark difference from weathered PE, PP, and PS, where IR spectroscopy revealed more weathering effects than Raman spectroscopy. Weathered PET exhibited a peak at approximately 3300 cm^{-1}, indicating the formation of OH groups, with more intense peaks observed in artificial seawater and Puget Sound seawater. The higher formation of OH groups in simulated marine weathering is consistent with other studies,[43,74] as hydrolysis is the primary degradation process of PET and results in carboxyl or hydroxyl-terminated end groups in the polymer chains.[74]

Uniquely, PET weathered in Puget Sound seawater showed increased IR intensity at 2920 cm^{-1} and 2852 cm^{-1} (C–H bending/stretching),[70,71] which was not observed in other weathering conditions. While requiring further investigation, this could potentially arise from the breakdown of phosphite antioxidants

Table 2 Selected Raman peaks and associated vibrational modes of PET

Peak position (cm^{-1})	Vibrational mode	Phase or associated features
3083, 3068, 3000	Ring C–H stretch (benzene ring)[64,65]	Orientation of species perpendicular to the polymer chain
2964	$–CH_2–$ groups adjacent to O atoms[64,65]	—
1725	C═O stretch[29,64,65,67]	Crystalline
1615	C–C/C═C symmetric stretch (1,4 carbons in benzene ring)[29,64,65,67]	Orientation of the polymer backbone chain
1451	CH_2 and OCH bending[65]	—
1413	CCH bending and OCH bending[65]	—
1370	CH_2 wag/bend[64]	—
1352	Ring breathing modes of sp^2 carbon[63]	—
1285	C–C ring stretch, C–O stretching[64,65]	—
1179	Ring C–H in plane bend, C–C stretch[64,65]	—
1120	Ring C–H in-plane bend, ester C(O)–O, *gauche* ethylene glycol C–C stretch[29,64]	—
1105, 1129	Ester C(O)–O, ethylene glycol C–C stretching[69]	—
1097	C–O, C–C stretch, ring C–C, ester C(O)–O, *trans* ethylene glycol C–C stretching[29]	Crystalline
890	CH_2 rocking[64]	—
860	C–C, C–O–C bend, ring C–C breathing (A_g mode), ester C(O)–O stretch[29]	—
853	C−C stretch (ring breathing), C−O stretch[64]	—
797	Ring C–H out-of-plane bend[64]	—
632	Ring CCC in plane bend[64]	—

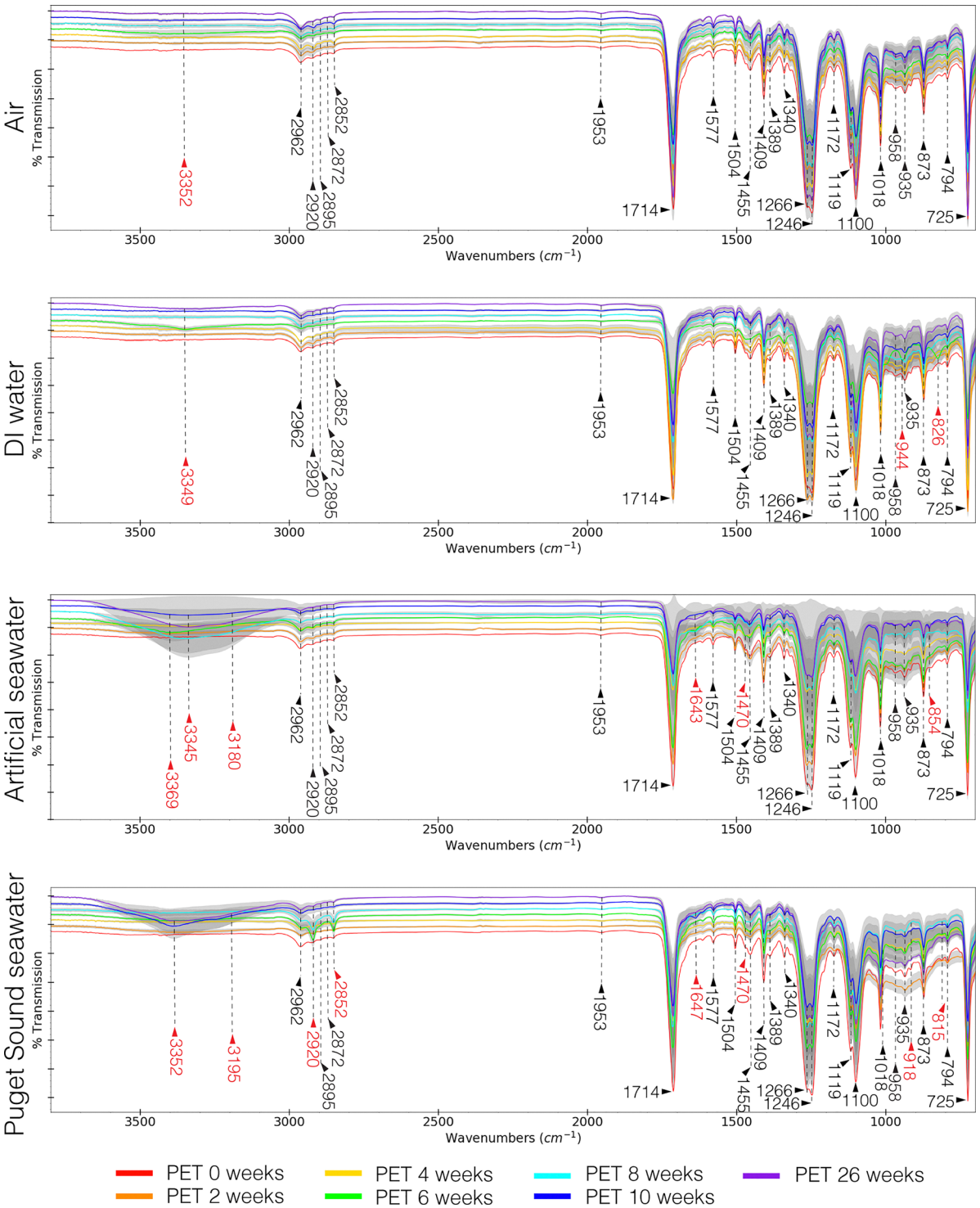

Fig. 4 Average IR spectra and standard deviation (grey error bands) of PET over time in four different weathering conditions in a staggered overlay. Red peaks are new IR peaks that differ from pristine PET.

commonly used in PET (unlike phenolic antioxidants, which cause discoloration).[75] Indeed, characteristic peaks for such additives (*e.g.*, C–H stretches ~2900 cm^{-1}, $-SO_3^-$ ~1242 cm^{-1}) are visible in our spectra (Fig. 4). The presence of these stabilizers might also explain the relatively minor IR spectral changes observed for PET overall compared to PS.

In contrast to PE, PP, and PS, the quantification of carbonyl content as a result of the weathering of PET is not as straightforward because of the inherent presence of the ester C=O stretch at 1714 cm^{-1}.[76] A combination of factors is associated with the intensity of the 1714 cm^{-1} peak; a decrease in absorbance intensity indicates ester bond scission, while an

Table 3 Selected IR peaks and associated vibrational modes of PET

Peak position (cm^{-1})	Vibrational mode	Weathering condition			
		Air	DI	AS	PSS
3550–3220[a]	O–H stretch[57]	×	×	×	×
2962, 2920,[a] 2895, 2852[a]	Aliphatic C–H stretch, CH_2 stretch[70,71]				×
1714	C═O stretch, aromatic ester[72]	×	×	×	×
1685	C═O (CO, CO_2, –COOH end group)[72]	×	×	×	×
1645[a]	–COOH[72]			×	×
1577, 1504	C═C ring stretch, ═C–H ring in-plane bend[70,71]	×	×	×	×
1470[a]	CH_2 bend, *trans*[71]		×		×
1455	CH_2 bend, O–CH bend[70]	×	×	×	×
1409	Phenylene in-plane ring deformation[70,72]	×	×	×	×
1370, 1340	CH_2 wag *cis*, CH_2 wag *trans*[70,71]	×	×	×	×
1266	C–O stretch carbonyl, ═C–C ring ester stretch, C═O in plane bend[71]	×	×	×	×
1172	═C–H ring in-plane bend, C═C ring stretch[71]	×	×	×	×
1100	C–O–C stretch, asymmetric methylene group stretch[70,73]	×	×	×	×
944[a]	Unknown		×		
873	═C–H ring out-of-plane bend, ═C–C ring ester out-of-plane bend, C═O out-of-plane bend, ring torsion[71]	×	×	×	×
815–854,[a] 918[a]	Unknown		×	×	×
725	═C–H ring out-of-plane bend, –C═O out-of-plane bend[70,71]	×	×	×	×

DI = deionized water, AS = artificial seawater, PSS = Puget Sound seawater. [a] Indicates peak changes.

increase indicates the formation of carbonyl-containing degradation products. When normalized to the phenylene ring vibrational reference peak at 1410 cm^{-1}, which is independent of polarization and sample orientation,[72,77] the absorbance intensity of the 1714 cm^{-1} peak slightly decreases over time in all weathering conditions (Fig. S10). Puget Sound seawater-weathered PET also shows a decrease in the 1714 cm^{-1} intensity from 0 to 10 weeks, but at 26 weeks, the CI is similar to pristine PET, which may indicate flaking of weathered PET over time.

In more detail, the aromatic-containing main chain of PET absorbs UV radiation during photodegradation, inducing chain scission of the ester bonds in the backbone and leading to a decrease in molecular weight and oxidation. This process proceeds through Norrish type I (which involves radical formation and cleavage of the α C–C bond adjacent to the carbonyl) and II (which involves intramolecular hydrogen abstraction from a γ carbon to a carbonyl oxygen) reactions to form carbonyl and carboxyl-containing products.[66,72,74,78]

To assess weathering by accounting for both ester bond scission and the formation of new carboxylic acid groups, the CI for PET is calculated from the ratio of the degradation product peak at 1685 cm^{-1} to the original ester peak at 1714 cm^{-1}, as shown in eqn (2):[72,79,80]

$$CI_{PET} = \frac{A_{1714}}{A_{1685}} \quad (2)$$

Spectral deconvolution resolved the overlapping absorbance in the carbonyl region to distinguish the ester and carboxylic groups. With increasing light exposure, the CI slightly increased in the air weathering condition and the CI decreased in the water weathering conditions (Fig. S11). Water promotes the hydrolysis of PET, and it is unsurprising that when weathered in water, it undergoes ester bond cleavage more readily than when weathered in air. The results also indicate the accumulation of oxidative degradation products in air-weathered PET. For PET weathered in artificial seawater and air, after 26 weeks, the CI was comparable to pristine samples. This may be an indication of flaking of the plastic surface to expose new, less weathered surfaces, followed by further degradation. In some cases, PET weathered in artificial seawater and Puget Sound seawater produced large peaks at 1645 cm^{-1}, indicative of acid-terminated hydrolysis products[72] that obscured the 1685 cm^{-1} peak completely and made it challenging to accurately determine the CI.

Nylon 6

Polyamide 6 (PA6), also known as Nylon 6, is a prevalent microplastic in wastewater and fishing gear, yet its weathering ratios are not well-established.[81,82] Our Raman analysis showed that weathered PA6 exhibited its most significant changes at 1081 cm^{-1} (C–C skeletal stretch), 1444 cm^{-1} (CH_2 bend), and 1637 cm^{-1} (C═O stretch) (Fig. 5 and Table 4). Notably, we found that PA6 weathered in water conditions exhibited more variation in these peaks than samples weathered in air. These variations indicate changes to the polymer backbone, likely due to oxygenated radicals reacting with the C–N peptide bond to initiate chain scission and form new carbonyl groups.[83,84]

As an initial examination, the 1637 cm^{-1} peak (amide I C═O stretch) was monitored to calculate a Raman CI (Fig. S12). The analysis showed that samples weathered in air, artificial seawater, and Puget Sound seawater exhibited an increase in this peak, followed by a decrease, with 26 week samples showing similar levels to pristine PA6. Samples in DI water, however, showed no specific trend. This lack of a clear trend corroborates findings by Fernández-González *et al.*, who also found that weathered PA6 spectral bands showed no trend over time.[82]

To further probe changes in PA6's complex crystalline structure at the surface, we tracked the intensity ratio of the 1081 cm^{-1} (associated with the γ-phase) and 1062 cm^{-1} (associated with all phases) peaks as a first-order approximation (Fig. S13). This ratio increased over time in air and Puget Sound seawater but decreased

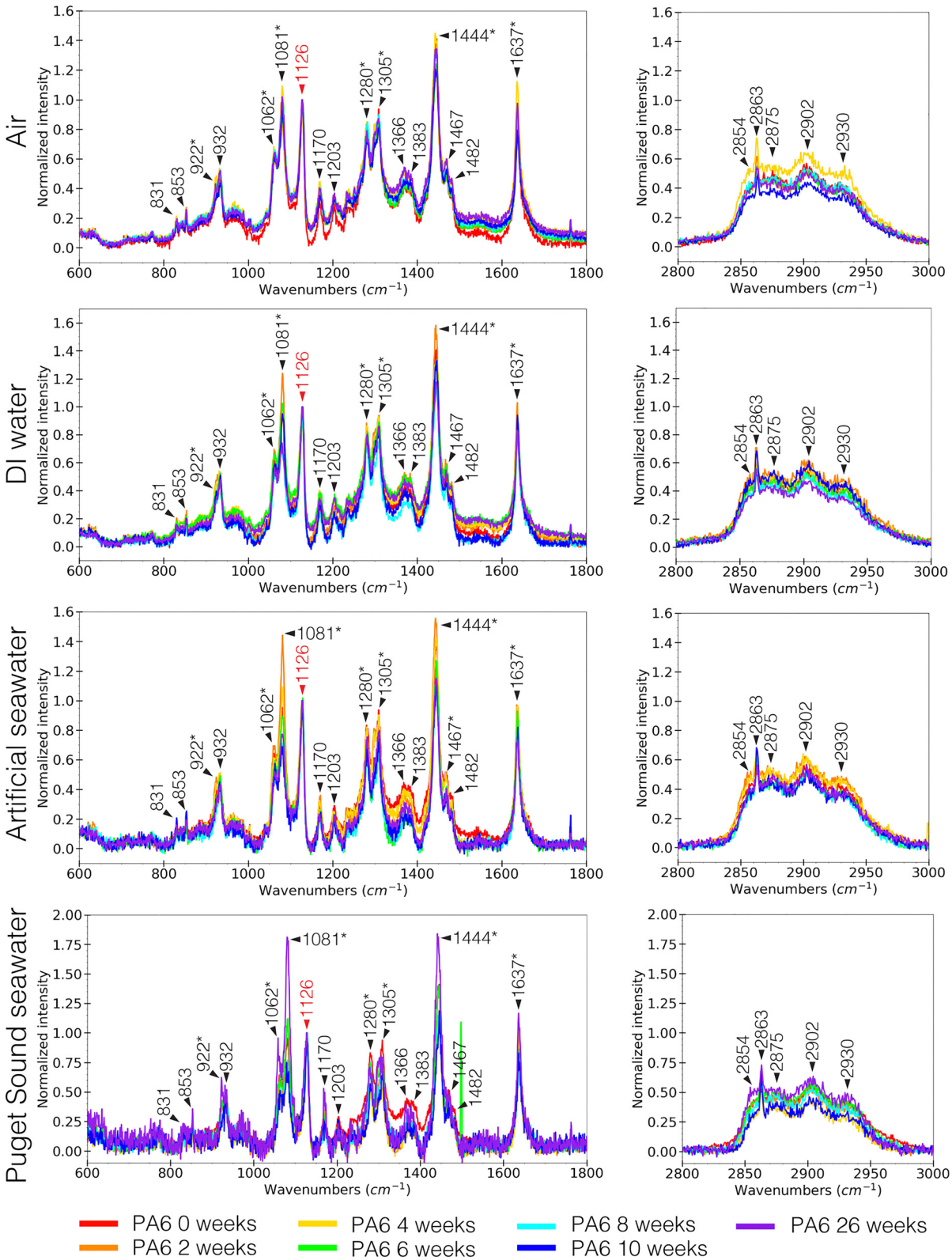

Fig. 5 Truncated Raman spectra highlighting the PA6 Raman spectral regions that exhibit the greatest normalized variability over time and in different weathering conditions (air, DI water, artificial seawater, and Puget Sound seawater). Red peak was used in spectral normalization. Asterixis-marked peaks showed the most observable changes.

over time in DI and AS. This suggests that when PA6 is weathered in air and Puget Sound seawater, the percentage of the γ-phase increases, implying the C–C sections of the backbone adopt more *gauche* configurations.

Table 4 Selected Raman peaks and associated vibrational modes of PA6

Peak position (cm^{-1})	Vibrational mode	Phase or associated features
2930	C–H stretch[85]	—
1637	C═O stretch[85–87]	Amide I
1467, 1480	C–N stretch, N–H bend[30,86,88]	Amide II, α-phase
1444	CH_2 bend[85,86]	—
1370	CH_2 wag[86]	—
1305	CH_2 twist[85,89]	β-phase
1280	C–N stretch, N–H bend[85,86]	Amide III
1126	C–C stretch[30]	Brill transition
1081 (main), 1060, 1121	C–C stretch[86–89]	All-*gauche* CC backbone, γ-phase
1062, 1080, 1127	C–C stretch[86,88,89]	Mesomorphic, β-phase
1063, 1075, 1129	C–C stretch[85,86]	All-*trans* CC backbone, α-phase
932	C–CO stretch, CO–NH in plane[85,88,89]	α-Phase
925	CO–NH in plane[89]	γ-Phase
833	CH_2 rock[90]	α-Phase

When examining weathered PA6 using IR, most identifying peaks were still present across the weathering conditions, although in some samples, weathering bands attributed to OH and C–O formation did develop. PA6 weathered in air showed very few formations of new IR spectral peaks, while samples in DI water showed more unique peaks not found in the other weathering conditions from 1417 cm^{-1} to 726 cm^{-1} (Fig. 6). Puget Sound seawater weathered samples showed the formation of bands around 3335 cm^{-1} (OH stretch), 1732 cm^{-1} (C═O stretch), and 1106 cm^{-1} (Table 5). All weathering conditions resulted in PA6 exhibiting a slight decrease in the 3081 cm^{-1} peak, which is assigned to the N–H deformation and C–N stretch.

The CI of PA6 can be calculated by the IR absorbance ratio of the C═O stretch, at 1637 cm^{-1}, and a reference peak. Reference peaks are selected based on their independence of chemical changes, and for PA6, this is the peak associated with the Brill transition at 1124 cm^{-1}.[82] However, because of the overlapping spectral peaks arising from weathering that occur in this region, deconvolution of the peak at 1124 cm^{-1} was not possible.

Interestingly, similar to PS, PA6 weathered in artificial seawater and Puget Sound seawater did not produce as many new IR peaks. The salt in these two weathering conditions may hinder the degradation effects of PA6 in a similar manner to PS, where reactive chlorine radicals ($Cl_2^{\bullet-}$) quench perhydroxyl radicals ($HO_2^{\bullet}$).[45] In terms of PA6, the chlorine radicals may disrupt other reactive oxygen species, such as OH and $O_2^{\bullet-}$, that contribute to the degradation process.[94] This is an interesting finding as aquaculture and fishing regularly utilize PA in their equipment, and our findings suggest there is more to understand about the photodegradation of lost fishing lines, also known as ghost fishing, in the marine environment. Previous work found that PA6 could not be degraded by microorganisms and will generally remain in the environment until they are photooxidized and mechanically crushed into microplastics.[95]

Differences in plastic type and weathering conditions

The weathering of PS, PET, and PA6 microplastics in different conditions demonstrates the differences in the chemical changes that can occur in the environment. Previous work found that these weathered PE and PP exhibited the most evident spectral changes when exposed to Puget Sound seawater, which suggested a difference in degradation pathways between laboratory simulations and environmental weathering.[15] Additionally, Raman spectroscopy revealed fluctuations in the crystalline phases of PE and PP, while IR spectroscopy provided more information about microplastic degradation products.[15]

Comparing these findings reveals key polymer-specific behaviors. Unlike PE and PP, PS showed stability in its Raman spectra under all conditions, while its IR spectra were altered by oxidation, especially in DI water, where unique byproducts formed. PET primarily showed increased structural disorder (D-band) *via* Raman, particularly in water, and accumulated more oxidative byproducts (IR) when weathered in air. PA6, like PS, was relatively stable but also produced more unique IR peaks in DI water compared to seawater. The contrasting effect of seawater on PE and PP compared to more functional group containing polymers such as PS, PET, and PA6 highlights the complex interplay between polymer structure and environmental chemistry. These distinct pathways underscore the need for polymer-specific analyses and the use of complementary spectroscopic techniques (Table 6). While bulk factors such as Flory–Huggins or Hansen solubility parameters are often used to describe polymer–solvent interactions, they do not account for the non-linear trends observed here. For instance, PE and PP would be expected to degrade less in seawater due to their hydrophobicity and yet they show significant spectral change.

It is important to note that complementary spectroscopic techniques, such as IR and Raman, have challenges and limitations when used in environmental microplastic analysis. These spectroscopic techniques support each other in confirming the identification of weathered microplastics and can provide microplastic researchers with information on some properties of the weathered materials found in the environment. While laboratory conditions can be easily controlled and manipulated, they do not truly reflect the degree of interaction that microplastics undergo in the environment. Therefore, it is important that laboratory experiments take into consideration multiple interacting factors that influence weathering.

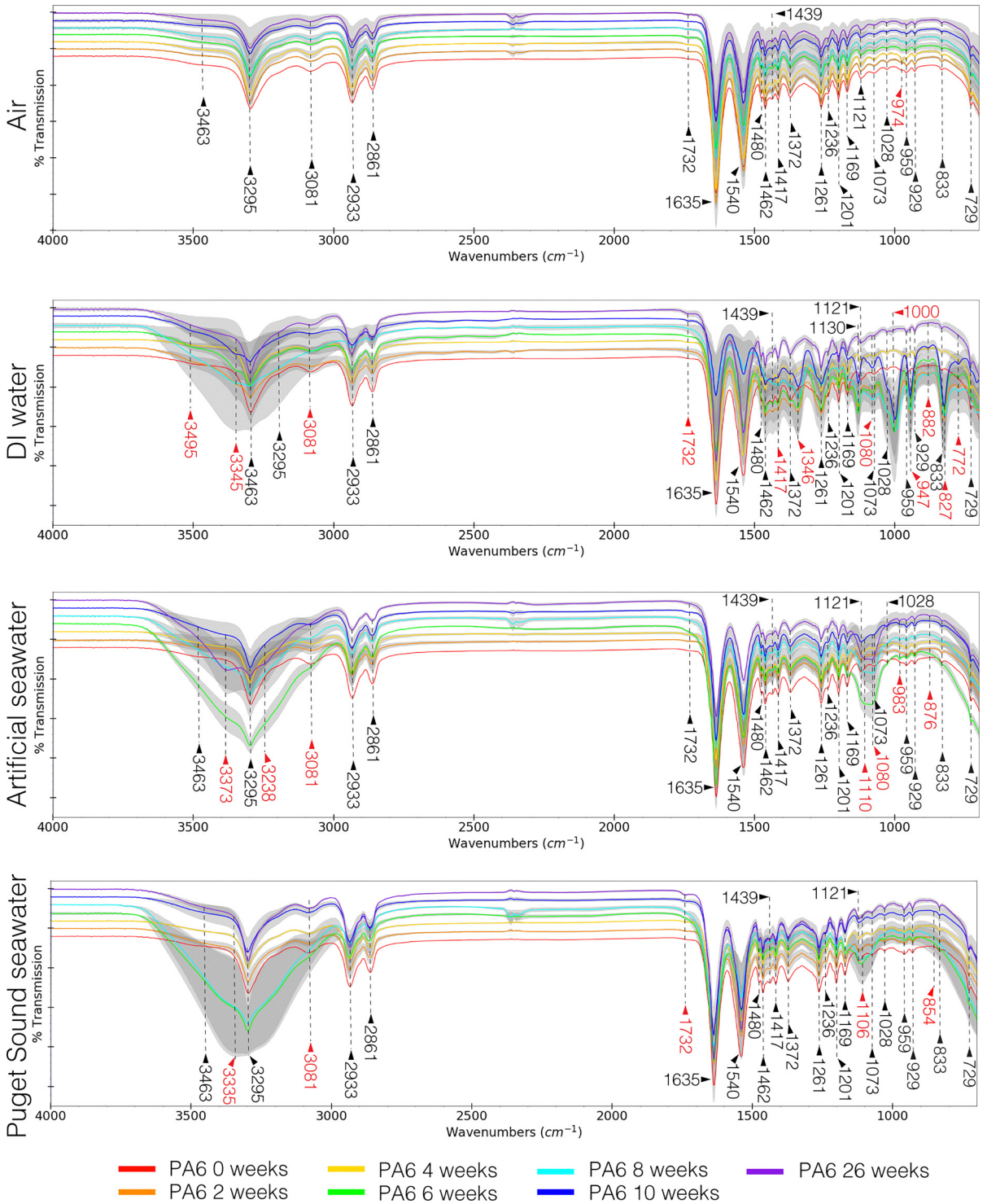

Fig. 6 Average IR spectra and standard deviation (grey error bands) of PA6 over time in four different weathering conditions in a staggered overlay. Red peaks are new IR peaks that differ from pristine PA6.

Additional techniques, such as DSC or XRD, should be integrated into future workflows to bridge the gap between surface-level spectral observations and bulk morphological transitions, to provide a more holistic understanding of the origin of these weathered structural changes.

Conclusions

This study compared the weathering effects of air and three different water environments (DI water, artificial seawater, and Puget Sound seawater) on PS, PET, and PA6 *via* Raman and IR spectroscopy. Our

Table 5 Selected IR peaks and associated vibrational modes of PA6

Peak position (cm^{-1})	Vibrational mode	Weathering condition			
		Air	DI	AS	PSS
3550–3220[a]	O–H stretch[57]		×	×	×
3295	N–H stretch, amide II[91,92]	×	×	×	×
3081[a]	N–H stretch[92]	×	×	×	×
2933	Symmetric CH_2 stretch[91,92]	×	×	×	×
2860	Asymmetric CH_2 stretch[91,92]	×	×	×	×
1732	C═O stretch, imides[83,93]	×	×	×	×
1635	C═C stretch, amide 1[91,93]	×	×	×	×
1540	N–H bend, amide II[91,93]	×	×	×	×
1417[a]	CH_2 scissor[92]		×		
1372	CH_2 wag, amide III[92]	×	×	×	×
1261	N–H bend, C–N stretch[92]	×	×	×	×
1201[a]	CH_2 twist-wag, α-phase[92]	×	×	×	×
1169	CO–NH skelal[90]	×	×	×	×
1080[a]	Unknown, γ-phase[90]		×	×	
1073	C–C stretch[90]	×	×	×	×
959, 950, 929	CO–NH in plane, α-phase[90,92]	×	×	×	×
726–983[a]	Unknown		×	×	
833	CH_2 rock, α-phase[90]	×	×	×	×

DI = deionized water, AS = artificial seawater, PSS = Puget Sound seawater. [a] Indicates peak changes.

Table 6 Summary of IR and Raman spectroscopy for PS, PET, and PA6 identification

	IR	Raman
PS	No major changes observed in air weathering; water conditions showed multiple weathering bands; water weathering effects can obscure identifying peaks	No change; all identifying peaks observable
PET	Observation of broad OH band formation; identifying peaks still observable	Formation of peak around 1352 cm^{-1}
PA6	Observation of broad OH band and presence of some peak formations in the fingerprint region	Identifying peaks are observable, though peak intensity may differ

work shows that spectral changes of weathered plastics often do not follow a linear progression with time, presenting challenges for the reliable identification of microplastics and their aging state. For example, Raman spectroscopy failed to detect the oxidation in PS that was visible by IR. Accurate assessment requires understanding these polymer-specific spectral changes leveraging the combined strengths of both Raman and IR spectroscopy. Considering the various global environmental conditions that microplastics are subjected to, the weathering effects can vary drastically. Future work will involve expanding spectral libraries and developing predictive models for spectral changes to improve identification accuracy in environmental samples.

Author contributions

S. Phan: conceptualization, data curation, formal analysis, investigation, methodology, software, validation, visualization, writing – original draft, and writing – review and editing. J. J. Ramtahal: writing – review and editing. C. K. Luscombe: conceptualization, funding acquisition, supervision, and writing – review and editing.

Conflicts of interest

The authors declare that they have no known competing financial interests or personal relationships that could have appeared to influence the work reported in this paper.

Data availability

Data for this article, including Raman and IR spectra for PS, PET, and PA6, are available at GitHub at https://github.com/samphan10/weathering.

Supplementary information (SI): representative IR and Raman spectra of PS, PET, and PA6, and carbonyl index analyses are included. See DOI: https://doi.org/10.1039/d5sm01102g.

Acknowledgements

The authors would like to thank V. Truong for assisting with literature searches for PET, Prof. J. L. Padilla-Gamiño for allowing us to use a Ni10 ThermoFisher IR microspectrometer, and the Nanofabrication section of Core Facilities at the Okinawa Institute of Science and Technology Graduate University for allowing us to use a WiTec alpha300 Apyron Raman microspectrometer. Part of this work was conducted at the Molecular Analysis Facility, a National Nanotechnology Coordinated Infrastructure site at the University of Washington, supported in part by the National Science Foundation (grant NNCI-1542101 and NNCI-2025489), the University of Washington, the Molecular Engineering & Sciences Institute, and the Clean Energy Institute. This work was also financially supported by the Okinawa Institute of Science and Technology Graduate University, the OIST Innovation Proof of Concept Program, and JSPS KAKENHI Grant Number JP24K20940.

Notes and references

1 R. Geyer, J. R. Jambeck and K. L. Law, Production, use, and fate of all plastics ever made, *Sci. Adv.*, 2017, **3**, e1700782.

2 A. L. Andrady, Microplastics in the marine environment, *Mar. Pollut. Bull.*, 2011, **62**, 1596–1605.

3 M. Cole, P. Lindeque, C. Halsband and T. S. Galloway, Microplastics as contaminants in the marine environment: a review, *Mar. Pollut. Bull.*, 2011, **62**, 2588–2597.

4 J. C. Martinelli, S. Phan, C. K. Luscombe and J. L. Padilla-Gamiño, Low incidence of microplastic contaminants in Pacific oysters (*Crassostrea gigas* Thunberg) from the Salish Sea, USA, *Sci. Total Environ.*, 2020, **715**, 136826.

5 L. S. T. Harris, S. Phan, D. DiMarco, J. L. Padilla-Gamiño, C. Luscombe and E. Carrington, Microparticles in marine mussels at regional and localized scales across the Salish Sea, Washington, *Mar. Pollut. Bull.*, 2023, **196**, 115609.

6 J. J. Ramtahal, K. Sugimoto, S. Phan, Tara Jambio Microplastic Consortium, Y. Patouillet, R. Troublé, C. K. Luscombe and S. Agostini, An integrated assessment of microplastic pollution in coastal surface water and sediment of Japan, *Environ. Sci. Technol.*, 2025, **59**, 17746–17759.

7 K. Blackburn and D. Green, The potential effects of microplastics on human health: what is known and what is unknown, *Ambio*, 2022, **51**, 518–530.

8 K. Munno, H. De Frond, B. O'Donnell and C. M. Rochman, Increasing the accessibility for characterizing microplastics: introducing new application-based and spectral libraries of plastic particles (SLoPP and SLoPP-E), *Anal. Chem.*, 2020, **92**, 2443–2451.

9 W. Cowger, Z. Steinmetz, A. Gray, K. Munno, J. Lynch, H. Hapich, S. Primpke, H. De Frond, C. Rochman and O. Herodotou, Microplastic spectral classification needs an open source community: open specy to the rescue!, *Anal. Chem.*, 2021, **93**, 7543–7548.

10 S. B. Borrelle, J. Ringma, K. L. Law, C. C. Monnahan, L. Lebreton, A. McGivern, E. Murphy, J. Jambeck, G. H. Leonard, M. A. Hilleary, M. Eriksen, H. P. Possingham, H. De Frond, L. R. Gerber, B. Polidoro, A. Tahir, M. Bernard, N. Mallos, M. Barnes and C. M. Rochman, Predicted growth in plastic waste exceeds efforts to mitigate plastic pollution, *Science*, 2020, **369**, 1515–1518.

11 K. Zhang, A. H. Hamidian, A. Tubić, Y. Zhang, J. K. H. Fang, C. Wu and P. K. S. Lam, Understanding plastic degradation and microplastic formation in the environment: A review, *Environ. Pollut.*, 2021, **274**, 116554.

12 X. Wu, X. Chen, R. Jiang, J. You and G. Ouyang, New insights into the photo-degraded polystyrene microplastic: Effect on the release of volatile organic compounds, *J. Hazard. Mater.*, 2022, **431**, 128523.

13 L. Liu, M. Xu, Y. Ye and B. Zhang, On the degradation of (micro)plastics: degradation methods, influencing factors, environmental impacts, *Sci. Total Environ.*, 2022, **806**, 151312.

14 B. Gewert, M. M. Plassmann and M. Macleod, Pathways for degradation of plastic polymers floating in the marine environment, *Environ. Sci.: Process. Impacts*, 2015, **17**, 1513–1521.

15 S. Phan, J. L. Padilla-Gamiño and C. K. Luscombe, The effect of weathering environments on microplastic chemical identification with Raman and IR spectroscopy: Part I. polyethylene and polypropylene, *Polym. Test.*, 2022, **116**, 107752.

16 S. Phan, D. Torrejon, J. Furseth, E. Mee and C. Luscombe, Exploiting weak supervision to facilitate segmentation, classification, and analysis of microplastics (<100 μm) using Raman microspectroscopy images, *Sci. Total Environ.*, 2023, **886**, 163786.

17 Y. Liu, W.-Y. Jiang, Y. Liao, R. Sun, J. Hu, Z. Lu, M. Chang, J. Yang, Z. Dai, C. Zhou, P. Hong, Z.-J. Qian, S. Sun, L. Ren, Y.-Q. Liang, Y. Zhang and C. Li, Separation of false-positive microplastics and analysis of microplastics via a two-phase system combined with confocal Raman spectroscopy, *J. Hazard. Mater.*, 2022, **440**, 129803.

18 Y. Liu, L. Lin, B. Yang, M. Huang, X. Huang, X. Chen, Z. Dai, S. Sun, Y. Yang and C. Li, Separation and identification of nanoplastics via a two-phase system combined with surface-enhanced Raman spectroscopy, *ACS Sustainables Chem. Eng.*, 2024, **12**, 1595–1604.

19 S. Walker, H. N. Mozaria-Luna, I. Kaplan and D. Petatán-Ramírez, Future temperature and salinity in Puget Sound, Washington State, under CMIP6 climate change scenarios, *J. Water Clim. Change*, 2022, **13**, 4255–4272.

20 Puget Sound's physical environment | Encyclopedia of Puget Sound. https://www.eopugetsound.org/articles/puget-sounds-physical-environment (accessed 29 October 2025).

21 Changes in Puget Sound Waters Over the Last Century | LiveOcean. https://faculty.washington.edu/pmacc/LO/long_term_trends.html (accessed 29 October 2025).

22 Puget Sound Water Temperature | WaterTemperature.net. https://www.watertemperature.net/united-states/puget-sound-water-temperature.html (accessed 29 October 2025).

23 M. O. Reese, A. M. Nardes, B. L. Rupert, R. E. Larsen, D. C. Olson, M. T. Lloyd, S. E. Shaheen, D. S. Ginley, G. Rumbles and N. Kopidakis, Photoinduced degradation of polymer and polymer–fullerene active layers: experiment and theory, *Adv. Funct. Mater.*, 2010, **20**, 3476–3483.

24 S. Holliday and C. K. Luscombe, Low boiling point solvent additives for improved photooxidative stability in organic photovoltaics, *Adv. Electron. Mater.*, 2018, **4**, 1700416.

25 Z.-M. Zhang, S. Chen and Y.-Z. Liang, Baseline correction using adaptive iteratively reweighted penalized least squares, *Analyst*, 2010, **135**, 1138–1146.

26 N. Brun, I. Youssef, M. C. Chevrel, D. Chapron, C. Schrauwen, S. Hoppe, P. Bourson and A. Durand, *In situ* monitoring of styrene polymerization using Raman spectroscopy. Multi-scale approach of homogeneous and heterogeneous polymerization processes, *J. Raman Spectrosc.*, 2013, **44**, 909–915.

27 N. Brun, M.-C. Chevrel, L. Falk, S. Hoppe, A. Durand, D. Chapron and P. Bourson, Contribution of Raman spectroscopy to *in situ* monitoring of a high-impact polystyrene process, *Chem. Eng. Technol.*, 2014, **37**, 275–282.

28 E. Perret, K. Chen, O. Braun, R. Muff and R. Hufenus, Radial gradients in PET monofilaments: a Raman mapping and SAXS tomography study, *Polymer*, 2022, **238**, 124422.
29 E. Perret, O. Braun, K. Sharma, S. Tritsch, R. Muff and R. Hufenus, High-resolution 2D Raman mapping of mono- and bicomponent filament cross-sections, *Polymer*, 2021, **229**, 124011.
30 D. Bertoldo Menezes, A. Reyer and M. Musso, Analysis of the Brill transition and reversible Brill transition in Nylon 6,6 by Raman spectroscopy, *Spectroscopy*, 2016, **31**, 44–48.
31 L. Puppulin, W. Zhu, N. Sugano and G. Pezzotti, Microstructural modifications induced by accelerated aging and lipid absorption in remelted and annealed UHMWPEs for total hip arthroplasty, *J. Biomater. Appl.*, 2015, **29**, 291–800.
32 A. Tagliaferro, M. Rovere, E. Padovano, M. Bartoli and M. Giorcelli, Introducing the novel mixed Gaussian–Lorentzian lineshape in the analysis of the Raman signal of biochar, *Nanomaterials*, 2023, **13**, 108.
33 Z. Kilinc, G. Yesilay, D. Cetin, Z. Suludere, S. Rashdan, L. Hazeem, M. Bououdina and G. Z. Kyzas, Photodegradation of polystyrene microplastics exposed to natural sunlight, *J. Photochem. Photobiol. A Chem.*, 2025, **468**, 116462.
34 J. Brandon, M. Goldstein and M. D. Ohman, Long-term aging and degradation of microplastic particles: comparing *in situ* oceanic and experimental weathering patterns, *Mar. Pollut. Bull.*, 2016, **110**, 299–308.
35 L. M. Hernandez, J. Grant, P. S. Fard, J. M. Farner and N. Tufenkji, Analysis of ultraviolet and thermal degradations of four common microplastics and evidence of nanoparticle release, *J. Hazard. Mater. Lett.*, 2023, **4**, 100078.
36 Y. Ikuno, H. Tsujino, Y. Haga, S. Manabe, W. Idehara, M. Hokaku, H. Asahara, K. Higashisaka and Y. Tsutsumi, Polyethylene, whose surface has been modified by UV irradiation, induces cytotoxicity: a comparison with microplastics found in beaches, *Ecotoxicol. Environ. Saf.*, 2024, **277**, 116346.
37 O. Changlake, P. Kaewkam, K.-Y. A. Lin, S. Sirivithayapakorn and K. Kobwittaya, Generation of biodegradable microplastics from commercially available PBAT and PLA-based plastic bags in water: impacts of UVA and water medium, *J. Hazard. Mater.*, 2025, **496**, 139207.
38 Depth Resolution of the Raman Microscope: Optical Limitations and Sample Characteristics. https://www.spectroscopyonline.com/view/depth-resolution-raman-microscope-optical-limitations-and-sample-characteristics (accessed 29 October 2025).
39 M. Hardy and H. O. M. Chu, Laser wavelength selection in Raman spectroscopy, *Analyst*, 2025, **150**, 1986–2008.
40 M. G. Nevins and J. N. Apell, Emerging investigator series: quantifying the impact of cloud cover on solar irradiance and environmental photodegradation, *Environ. Sci.: Impacts*, 2021, **23**, 1884.
41 E. Yousif and R. Haddad, Photodegradation and photostabilization of polymers, especially polystyrene: review, *SpringerPlus*, 2013, **2**, 1–32.
42 D. J. Carlsson and D. M. Wiles, The photodegradation of polypropylene films. III. Photolysis of polypropylene hydroperoxides, *Macromolecules*, 1969, **2**, 597–606.
43 V. Fernández-González, J. M. Andrade-Garda, P. López-Mahía and S. Muniategui-Lorenzo, Impact of weathering on the chemical identification of microplastics from usual packaging polymers in the marine environment, *Anal. Chim. Acta*, 2021, **1142**, 179–188.
44 Q. Wen, N. Liu, R. Qu and F. Ge, High salinity promotes the photoaging of polystyrene microplastics with humic acid in seawater, *Sci. Total Environ.*, 2023, **901**, 165741.
45 X. Wu, P. Liu, H. Wang, H. Huang, Y. Shi, C. Yang and S. Gao, Photo aging of polypropylene microplastics in estuary water and coastal seawater: Important role of chlorine ion, *Water Res.*, 2021, **202**, 117396.
46 K. Nishikida and J. Coates, *Handbook of Plastics Analysis: Infrared and Raman Analysis of Polymers*, CRC Press, 1st edition, 2003.
47 X. Wu, X. Chen, R. Jiang, J. You and G. Ouyang, New insights into the photo-degraded polystyrene microplastic: effect on the release of volatile organic compounds, *J. Hazard. Mater.*, 2022, **431**, 128523.
48 T. Lomonaco, E. Manco, A. Corti, J. La Nasa, S. Ghimenti, D. Biagini, F. Di Francesco, F. Modugno, A. Ceccarini, R. Fuoco and V. Castelvetro, Release of harmful volatile organic compounds (VOCs) from photo-degraded plastic debris: a neglected source of environmental pollution, *J. Hazard. Mater.*, 2020, **394**, 122596.
49 G. K. Gupta, M. Dixit, E. Chot and P. Shukla, Insights into microbial enzymatic biodegradation of plastics and microplastics: technological updates, *ACS Environ. Au*, 2025, **5**, 520–542.
50 P. Bonechi, I. Kandylioti, A. Cincinelli, I. A. Ionescu and E. Psillakis, Linear relationship between carbonyl index of weathered microplastics with a C–C backbone and solar light photodegradation kinetics of nicotine, *J. Photochem. Photobiol. A Chem.*, 2026, **470**, 116609.
51 V. Mylläri, T.-P. Ruoko and S. Syrjälä, A comparison of rheology and FTIR in the study of polypropylene and polystyrene photodegradation, *J. Appl. Polym. Sci.*, 2015, **132**, 42246.
52 H. Nakatani, Y. Ohshima, T. Uchiyama and M. Suguru, Degradation and fragmentation behavior of polypropylene and polystyrene in water, *Sci. Rep.*, 2022, **12**, 18501.
53 M. Dong, Q. Zhang, X. Xing, W. Chen, Z. She and Z. Luo, Raman spectra and surface changes of microplastics weathered under natural environments, *Sci. Total Environ.*, 2020, **739**, 139990.
54 N. Meides, A. Mauel, T. Menzel, V. Altstädt, H. Ruckdäschel, J. Senker and P. Strohriegl, Quantifying the fragmentation of polypropylene upon exposure to accelerated weathering, *Microplast. Nanoplast.*, 2022, **2**, 23.
55 H. Nakatani, T. Kyan and T. Muraoka, An effect of water presence on surface exfoliation of polypropylene film initiated by photodegradation, *J. Polym. Environ.*, 2020, **28**, 2219–2226.
56 H. Nakatani, T. Muraoka, Y. Ohshima and S. Motokucho, Difference in polypropylene fragmentation mechanism between marine and terrestrial regions, *SN Appl. Sci.*, 2021, **3**, 773.

57 P. J. Larkin, *Infrared and Raman Spectroscopy: Principles and Spectral Interpretation*, Elsevier Inc., 2011.
58 B. C. Smith, The infrared spectra of polymers III: hydrocarbon polymers, *Spectroscopy*, 2021, **36**, 22–25.
59 B. Smith, Distinguishing structural isomers: mono- and disubstituted benzene rings, *Spectroscopy*, 2016, **31**, 36–39.
60 V. Siipola, T. Tamminen, A. Källi, R. Lahti, H. Romar, K. Rasa, R. Keskinen, J. Hyväluoma, M. Hannula and H. Wikberg, Effects of biomass type, carbonization process, and activation method on the properties of bio-based activated carbons, *BioResources*, 2018, **13**, 5976–6002.
61 N. Labbé, D. Harper, T. Rials and T. Elder, Chemical structure of wood charcoal by infrared spectroscopy and multivariate analysis, *J. Agric. Food Chem.*, 2006, **54**, 3492–3497.
62 S. H. Park and S. H. Kim, Poly(ethylene terephthalate) recycling for high value added textiles, *Fashion Text.*, 2014, **1**, 1–17.
63 M. Veres, S. Tóth and M. Koós, New aspects of Raman scattering in carbon-based amorphous materials, *Diam. Relat. Mater.*, 2008, **17**, 1692–1696.
64 L. Bistričić, V. Borjanović, M. Leskovac, L. Mikac, G. E. McGuire, O. Shenderova and N. Nunn, Raman spectra, thermal and mechanical properties of poly(ethylene terephthalate) carbon-based nanocomposite films, *J. Polym. Res.*, 2015, **22**, 39.
65 E. Rebollar, S. Pérez, M. Hernández, C. Domingo, M. Martín, T. A. Ezquerra, J. P. García-Ruiz and M. Castillejo, Physicochemical modifications accompanying UV laser induced surface structures on poly(ethylene terephthalate) and their effect on adhesion of mesenchymal cells, *Phys. Chem. Chem. Phys.*, 2014, **16**, 17551–17559.
66 G. J. M. Fechine, R. M. Souto-Maior and M. S. Rabello, Structural changes during photodegradation of poly(ethylene terephthalate), *J. Mater. Sci.*, 2002, **37**, 4979–4984.
67 V. F. Alexiou, G. N. Mathioudakis, K. S. Andrikopoulos, A. S. Beobide and G. A. Voyiatzis, Poly(Ethylene terephthalate) carbon-based nanocomposites: a crystallization and molecular orientation study, *Polymers*, 2020, **12**, 2626.
68 A. J. Melveger, Laser-Raman study of crystallinity changes in poly(ethylene terephthalate), *J. Polymer Sci. Part A-2*, 1972, **10**, 317–322.
69 X. Zhao, Z. Zheng, I. M. Chou, M. Xiong and S. Mei, *In situ* experimental study on high-temperature hydrolysis of polyethylene terephthalate, *Polym. Eng. Sci.*, 2025, **65**, 4644–4652.
70 Z. Chen, J. N. Hay and M. J. Jenkins, FTIR spectroscopic analysis of poly(ethylene terephthalate) on crystallization, *Eur. Polym. J.*, 2012, **48**, 1586–1610.
71 C. Ricci, L. Gontrani, E. M. Bauer, G. Ciufolini, A. Lembo, L. Casoli and M. Carbone, Metal ion microwave-assisted depolymerization of poly(ethylene terephthalate): a zinc salts-based deep eutectic solvent as case study, *Crystals*, 2024, **14**, 567.
72 S. Rostampour, R. Cook, S. S. Jhang, Y. Li, C. Fan and L. P. Sung, Changes in the chemical composition of polyethylene terephthalate under UV radiation in various environmental conditions, *Polymers*, 2024, **16**, 2249.
73 A. P. dos Santos Pereira, M. H. Prado da Silva, É. P. Lima Júnior, A. dos Santos Paula and F. J. Tommasini, Processing and characterization of PET composites reinforced with geopolymer concrete waste, *Mater. Res.*, 2017, **20**, 411–420.
74 T. Sang, C. J. Wallis, G. Hill and G. J. P. Britovsek, Polyethylene terephthalate degradation under natural and accelerated weathering conditions, *Eur. Polym. J.*, 2020, **136**, 109873.
75 S. Sun, L. Wang, P. Song, L. Ding and Y. Bai, Facile fabrication of hydrolysis resistant phosphite antioxidants for high-performance optical PET films *via in situ* incorporation, *Chem. Eng. J.*, 2017, **328**, 406–416.
76 J. Bayo, D. Rojo and S. Olmos, Weathering indices of microplastics along marine and coastal sediments from the harbor of Cartagena (Spain) and its adjoining urban beach, *Mar. Pollut. Bull.*, 2022, **178**, 113647.
77 Y. Wang and S. Lehmann, Interpretation of the structure of poly(ethylene terephthalate) by dynamic FT-IR spectra, *Appl. Spectrosc.*, 1999, **53**, 914–918.
78 C. R. Hurley and G. J. Leggett, Quantitative investigation of the photodegradation of polyethylene terephthalate film by friction force microscopy, contact-angle goniometry, and X-ray photoelectron spectroscopy, *ACS Appl. Mater. Interfaces*, 2009, **1**, 1688–1697.
79 B. Du, R. Yang and X. M. Xie, Investigation of hydrolysis in poly(ethylene terephthalate) by FTIR-ATR, *Chin. J. Polym. Sci.*, 2014, **32**, 230–235.
80 M. Drobota, Z. Persin, L. F. Zemljic, T. Mohan, K. Stana-Kleinschek, A. Doliska, M. Bracic, V. Ribitsch, V. Harabagiu and S. Coseri, Chemical modification and characterization of poly(ethylene terephthalate) surfaces for collagen immobilization, *Cent. Eur. J. Chem.*, 2013, **11**, 1786–1798.
81 J. M. Lee, R. Busquets, I. C. Choi, S. H. Lee, J. K. Kim and L. C. Campos, Photocatalytic degradation of polyamide 66; evaluating the feasibility of photocatalysis as a microfibre-targeting technology, *Water*, 2020, **12**, 3551.
82 V. Fernández-González, J. M. Andrade, B. Ferreiro, P. López-Mahía and S. Muniategui-Lorenzo, Monitorization of polyamide microplastics weathering using attenuated total reflectance and microreflectance infrared spectrometry, *Spectrochim. Acta, Part A*, 2021, **263**, 120162.
83 S. Mouffok and M. Kaci, Artificial weathering effect on the structure and properties of polypropylene/polyamide-6 blends compatibilized with PP-g-MA, *J. Appl. Polym. Sci.*, 2015, **132**, 41722.
84 B. G. Achhammer, F. W. Reinhart and G. M. Kline, Mechanism of the degradation of polyamides, *J. Res. Natl. Bur. Stand.*, 1951, **46**, 2210.
85 D. Puchowicz and M. Cieslak, Raman spectroscopy in the analysis of textile structures, in *Recent Developments in Atomic Force Microscopy and Raman Spectroscopy for Materials Characterization*, IntechOpen, 2022, DOI: 10.5772/intechopen.99731.
86 H. Uematsu, T. Kawasaki, K. Koizumi, A. Yamaguchi, S. Sugihara, M. Yamane, K. Kawabe, Y. Ozaki and S. Tanoue, Relationship between crystalline structure of

polyamide 6 within carbon fibers and their mechanical properties studied using micro-Raman spectroscopy, *Polymer*, 2021, **223**, 123711.

87 J. S. Stephens, D. B. Chase and J. F. Rabolt, Electrospinning process on polymer crystallization chain conformation in Nylon-6 and Nylon-12, *Macromolecules*, 2004, **37**, 877–881.

88 A. Milani, Unpolarized and polarized Raman spectroscopy of Nylon-6 polymorphs: a quantum chemical approach, *J. Phys. Chem. B*, 2015, **119**, 3868–3874.

89 V. Ferreiro, C. Depecker, J. Laureyns and G. Coulon, Structures and morphologies of cast and plastically strained polyamide 6 films as evidenced by confocal Raman microspectroscopy and atomic force microscopy, *Polymer*, 2004, **45**, 6013–6026.

90 N. Vasanthan and D. R. Salem, FTIR spectroscopic characterization of structural changes in polyamide-6 fibers during annealing and drawing, *J. Polym. Sci. B: Polym. Phys.*, 2001, **39**, 536–547.

91 A. Dawelbeit and M. Yu, Tentative confinement of ionic liquids in Nylon 6 fibers: a bridge between structural developments and high-performance properties, *ACS Omega*, 2021, **6**, 3535–3547.

92 E. Rusu, G. Rusu and D.-O. Dorohoi, Thermal influence on structure of polymers with ε-caprolactam units studied by FT-IR spectroscopy, *Polimery*, 2009, **54**, 347–353.

93 D. Sedláček, M. Roso and A. P. Manian, The effect of a hydrophobic coating on the photodegradation of dyed Nylon 6 yarns, *Fibers Polym.*, 2023, **24**, 3889–3900.

94 Á. E. Rodríguez-Olivares, J. L. Guzmán-Mar, P. C. Quero-Jiménez, S. M. Montemayor, L. Maya-Treviño and L. Hinojosa-Reyes, Analytical approaches to track nylon 6 microplastic fiber degradation using HKUST-1(Cu/Fe)-derived CuO/TiO_2 photocatalyst, *J. Water Proc. Eng.*, 2025, **71**, 107192.

95 Y. An, T. Kajiwara, A. Padermshoke, T. Van Nguyen, S. Feng, H. Mokdai, T. Masaki, M. Takigawa, T. Van Nguyen, H. Masunaga, S. Sasaki and A. Takahara, Environmental degradation of nylon, poly(ethylene terephthalate) (PET), and poly(vinylidene fluoride) (PVDF) fishing line fibers, *ACS Appl. Polym. Mater.*, 2023, **5**, 4427–4436.